



Cite this: DOI: 10.1039/d5sc06960b

All publication charges for this article have been paid for by the Royal Society of Chemistry

Photochemical activation of pincer-ligated phosphoranides: mechanistic insight for reduction of aryl halides

Emile Escoudé,^a Manuel Pedrón,^b Lilian Bourqui,^b Geoffrey Gontard,^c Maxime R. Vitale,^a Ilaria Ciofini,^b Sami Lakhdar^b and Laurence Grimaud^{a*}

Pincer-ligated phosphoranides constitute a relatively underexplored subclass of main-group compounds whose distinctive structural and electronic properties are now attracting renewed interest. In this study, we report the synthesis, full characterization, and novel photoreactivity of O,N,O-pincer ligated phosphoranide anions. Upon visible-light irradiation, these species engage in single-electron transfer (SET) processes with various aryl halides, enabling the formation of C–P and C–C bonds. A combination of electrochemical studies and TD-DFT calculations supports a mechanism involving the formation of electron donor–acceptor (EDA) complexes, followed by light-induced SET and radical recombination. These findings introduce these phosphoranides as a versatile platform for photochemical transformations and underscore the broader potential of main-group frameworks in light-driven redox chemistry.

Received 9th September 2025

Accepted 21st October 2025

DOI: 10.1039/d5sc06960b

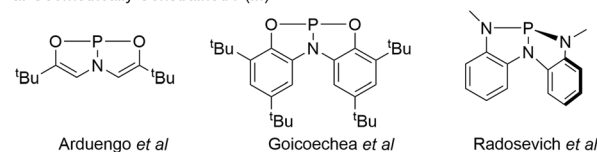
rsc.li/chemical-science

Introduction

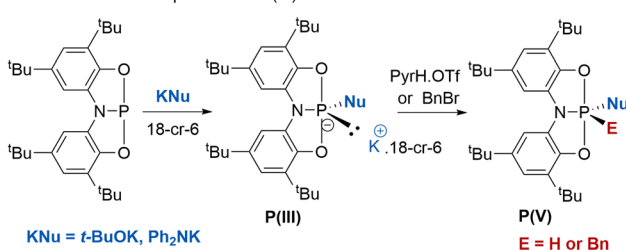
Trivalent phosphines (P(III)) featuring C_{3v} symmetry have long served as common nucleophiles,^{1–3} Lewis bases, and privileged ligands in organic synthesis, catalysis, and coordination chemistry. Their modularity has enabled decades of innovation, from transition-metal complex stabilization to small-molecule activation. Over the past several decades, efforts have increasingly focused on tuning their steric and electronic profiles to access new chemical reactivity, particularly through the development of unconventional phosphorus architectures. Among these, geometrically constrained phosphite P(III) species have emerged as a transformative subclass. Introduced by the pioneering work of Arduengo,^{4,5} these species enforce a constrained geometry at phosphorus that departs significantly from the canonical trigonal pyramidal structure (Fig. 1a). This structural deviation results in a marked decrease in HOMO–LUMO gap, fundamentally conferring ambiphilic reactivity.⁶ This unique electronic signature enables these P(III) to function not only as classical nucleophiles but also, and more strikingly,

as electrophilic centers,⁷ thereby challenging traditional views of P(III) chemistry.

a. Geometrically Constrained P(III)



b. Goicoechea's Phosphoranides P(III)



c. Constrained phosphoranide

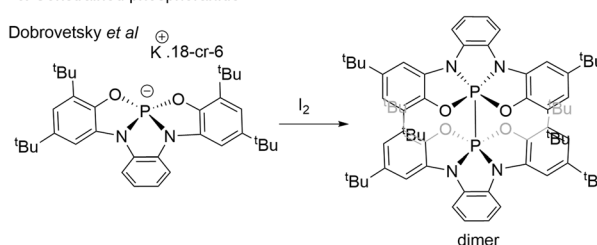


Fig. 1 Some constrained phosphites and related phosphoranides.

^aCPCV, Département de Chimie, École Normale Supérieure, PSL University, Sorbonne Université, CNRS, Paris, 75005, France. E-mail: laurence.grimaud@ens.psl.eu

^bPSL University, Chimie ParisTech, CNRS, Institute of Chemistry for Life and Health Sciences, F-75005 Paris, France. E-mail: ilaria.ciofini@chimieparistech.psl.eu

^cSorbonne Université, CNRS, Institut Parisien de Chimie Moléculaire, IPCM, F-75005 Paris, France

^dCNRS/Université Paul Sabatier, Laboratoire Hétérochimie Fondamentale et Appliquée (LHFA, UMR5069), 118 Route de Narbonne, 31062 Toulouse Cedex 09, France. E-mail: sami.lakhdar@utoulouse.fr

This dual reactivity has been convincingly demonstrated by Radosevich,^{8–10} Goicoechea,^{6,7,11,12} and others.^{13–17} Goicoechea, for instance, has shown that a prototypical constrained P(III) (**1**) undergoes rapid reaction with alkoxides or amides to generate isolable phosphoranide anions (**2**).⁷ These anionic P(III) species, fully characterized, offer unambiguous evidence of the latent electrophilicity in geometrically constrained phosphites. Upon treatment with common electrophiles, these anions can be cleanly converted into thermodynamically favored phosphoranes P(V) (**3**) (Fig. 1b). A similar reactivity was also observed more recently by Abbeneth and Goicoechea with a NNN acridane P(III).¹⁸

Recent contributions to the field of p-block chemistry further underscored the versatility of non-neutral phosphorus species.^{19–25} The work of Dobrovetsky on a constrained phosphoranide anion especially caught our attention.²⁶ His team prepared a potassium phosphoranide supported by a tetradentate O,O,N,N-ligand and stabilized it using 18-crown-6 (Fig. 1c). The resulting anionic species displayed nucleophilic substitution at phosphorus with iodomethane and oxidative dimerization with iodine (Fig. 1c), with an irreversible oxidation potential measured at $E_{\text{ox}}^{\text{P}} = 1.54 \text{ V}$ versus $\text{Ag}^+|\text{Ag}$. These results demonstrate not only the synthetic accessibility of these unusual anions but also their capacity for well-defined redox and substitution chemistry.

While the photochemistry of classical phosphorus anions has been elegantly explored, most notably in the seminal studies by Bunnett,²⁷ and Rossi^{28,29} on the photoinduced $\text{S}_{\text{RN}}1$ reactions of phosphorus anions with haloarenes (Fig. 2, top), and more recently in Li's transition-metal-free, photoinduced coupling of aryl halides with H-phosphonates,³⁰ the photo-reactivity of P(III) phosphoranide anions derived from geometrically constrained phosphoranes remains entirely uncharted. To date, no investigations have addressed how these structurally and electronically unique species respond to visible-light excitation. Given the presence of the aromatic pincer ligand, these phosphoranides are, in principle, ideally suited to participate in photoinduced electron transfer or radical-mediated transformations. We hypothesized that the aromatic pincer ligand could endow these anions with distinct

photophysical and photochemical properties, potentially unlocking reactivity inaccessible to either classical phosphines or phosphoranides (Fig. 2, bottom). Exploring the light-induced behavior of these species thus represents a critical and yet unexplored opportunity to expand the frontier of main group photochemistry.

Results and discussion

The constrained P(III) first reported by Goicoechea was selected due to its stability as no decoordination was observed when treated with various nucleophiles.⁷ The addition of cesium fluoride on the P(III) **1** led to the isolation of the corresponding fluoro-phosphoranide (Fig. 3). Single-crystal X-ray diffraction of the cesium salt in the presence of 18-crown-6 confirms the molecular structure, revealing an average P–F bond length of $1.63(2) \text{ \AA}$ —significantly longer than the 1.58 \AA observed in the PF_6^- anion (Fig. 3)—, which suggests that the Lewis adduct between the fluoride ion and the P(III) **1** is weaker than with PF_5 . Even if P(III) **1** is geometrically constrained, the geometry of the fluoro-phosphoranide is the one predicted by VSEPR theory, the lone pair of electrons occupying the fifth position of a trigonal bipyramid. The average N–P–F angles of $102.5(10)^\circ$ and O–P–F angles of $87(4)^\circ$, position the P–F bond nearly orthogonal to the ligand-defined coordination plane.

To form phosphoranides with enhanced covalent interactions, we screened different carbon-centered bases. From *tert*-butyllithium and P(III) **1** no product was detected by ^{31}P NMR. Addition of a large excess of N,N,N',N'-tetramethylethylenediamine (TMEDA) to the 1 : 1 mixture of **1** : $^t\text{BuLi}$ was required to observe complete consumption of **1** along with a new broad signal at 154.4 ppm by ^{31}P NMR. This signal pattern strongly correlated with the TMEDA concentration (refer to SI Section S3.1) suggesting the formation of lithium aggregates. In contrast, potassium phenylacetylide readily reacted with **1** in THF to give the corresponding phosphoranide **2a** as a yellow solid in 80% isolated yield (Fig. 4a). The characterization of **2a** by ^{31}P NMR proved that the signal is highly dependent on the solvent polarity as it sharpens and shifts from 31.5 ppm in

$\text{S}_{\text{RN}}1$ with phosphanides (Bunnett *et al*)

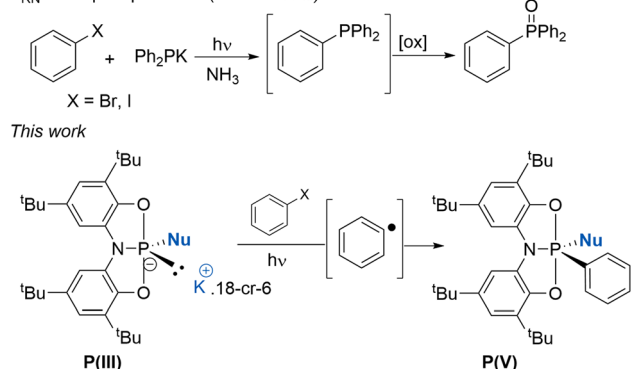


Fig. 2 Reactivity of phosphoranides under UV-Vis irradiation.

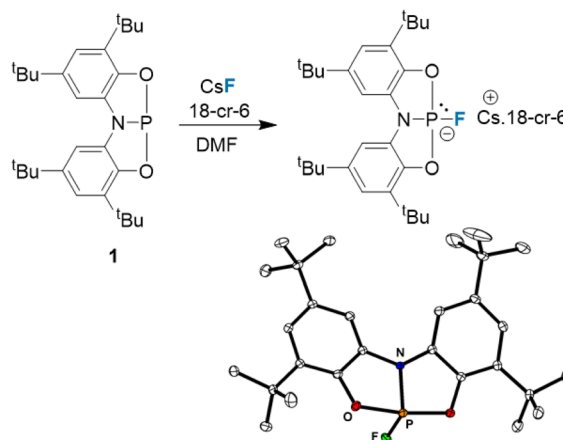


Fig. 3 Synthesis of fluoro phosphoranide.



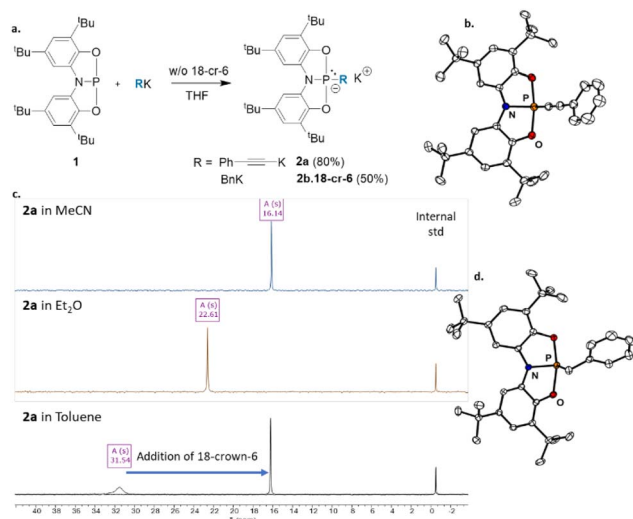


Fig. 4 Synthesis and characterization of **2a** and **2b**.

toluene to 16.1 ppm in acetonitrile (Fig. 4c), suggesting a strong interaction between the phosphoranide and the potassium cation in non-polar solvents. In the presence of 18-crown-6, the ^{31}P NMR chemical shift was almost independent of the solvent used (Fig. 4c). This ion-pairing was further confirmed by UV-Vis spectroscopy as a red-shift of 12 nm of the maximum of absorption of **2a** was observed upon addition of 18-crown-6 in THF (Fig. S112). X-Ray analyses of a monocrystal of the salt resulting from a 1:1 mixture of **2a** and **18-cr-6**, **2a.18-cr-6**, confirmed the structure of **2a** with the alkyne almost orthogonal to the plane defined by the P and its ligand as observed for the fluoro phosphoranide with an NPC_{sp} angle of 102.8° (Fig. 4b). The C–P bond is 1.81 Å long, which is in line with classical C–P bonds. Similarly, the benzyl phosphoranide **2b.18-cr-6** was synthesized in 50% isolated yield by treating **1** with benzyl potassium and **18-cr-6** (Fig. 4a) and characterized by a single peak at 68.9 ppm by $^{31}\text{P}\{^1\text{H}\}$ NMR spectrum in MeCN (see Section S2.2.e). The X-ray analysis of the crystals confirmed the structure of **2b.18-cr-6** and, as noted before, the P–Bn bond is almost orthogonal to the plane defined by P with an $\text{NPC}_{(\text{Bn})}$ angle of 99.3° and a C–P bond of 1.88 Å (Fig. 4d).

The redox behavior of both phosphoranides was investigated using cyclic voltammetry (CV) performed in DMF using $\text{NaBAR}_4^{\text{F}}$ as the supporting electrolyte. The CV of **2a** displays an irreversible oxidation wave at $E_{\text{p}/2} = -0.68 \text{ V vs. Fc}^+/\text{Fc}$ (Fig. 5, Section S7). In order to investigate the nature of the product resulting from its oxidation, phosphoranide **2a** was treated by 1 equiv of ferrocenium tetrafluoroborate in DMF at rt and the corresponding dimeric species **3a** was isolated in 33% yield (Fig. 5, bottom). A first anionic dimeric species derived from $\text{P}(\text{III}) **1** was previously isolated by Goicoechea when studying the reduction of **1** with KC_8 .⁷ However the dimer **3a** most likely results from the dimerization of the phosphoranide radical intermediate generated by oxidation of the anion as observed by Dobrovetsky.²⁶ Even if sterically hindered, this radical proved to be rather unstable as whatever the scan rate used for the CV, no$

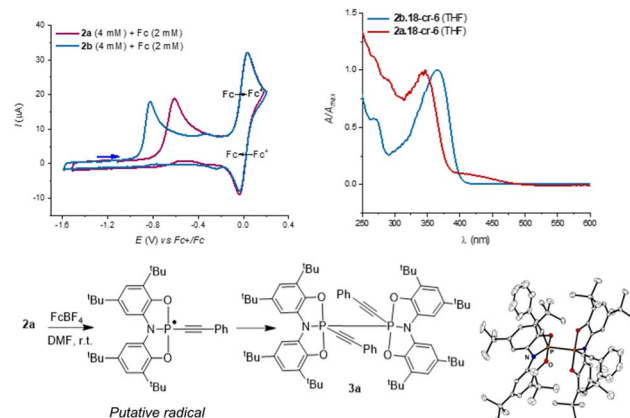


Fig. 5 Electrochemical and UV-vis characterization of **2a** and **2b** and study of the chemical oxidation of **2a**.

reversible electron transfer could be observed. Due to the irreversibility of the redox event, the oxidation potential of the excited state could only be estimated using the Rehm–Weller equation at *ca.* $-3.6 \text{ V vs. Fc}^+/\text{Fc}$ (see SI, Section S8). The oxidation potential of the excited state of **2b.18-cr-6** was then assessed. The UV-visible spectrum of **2b.18-cr-6** features a broad absorption band centered at 366 nm and the CV displays an irreversible oxidation wave at $E_{\text{p}/2} = -0.88 \text{ V vs. Fc}^+/\text{Fc}$. These data suggest that **2b.18-cr-6** in its excited state, should be a better reductant than excited **2a** as its oxidation potential would be at about $-4.0 \text{ V vs. Fc}^+/\text{Fc}$.

These results prompted us to explore the reducing properties of these phosphoranides under irradiation, in analogy to the behavior of phosphorous anions described by Bunnett,²⁷ and Rossi.^{28,29} To this end, we firstly turned to theoretical chemistry. The UV-Vis absorption spectrum of phosphoranide **2a** was computed at TD-DFT level, in the presence and absence of the potassium cation to simulate the influence of the addition of 18-crown-6 (reported in Fig. 6). In agreement with experiments, both spectra show two bands: an intense band in the UV (at 291 nm and 301 nm in presence or absence of K^+ cation), and

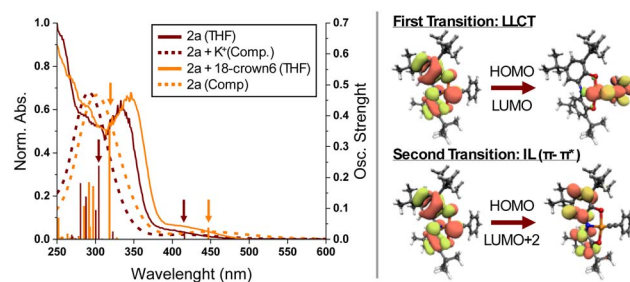


Fig. 6 (Left): experimental (solid line) and computed (dashed line) UV-Vis spectra of **2a** in the presence (**2a** + K^+) and absence (**2a**) of the K^+ . Oscillator strengths are represented as vertical lines and first and second transitions are marked with arrows of their respective color. (Right): isocontour representation of the orbitals mainly involved in the first two electronic transitions (isovalue 0.03 a.u.) computed for **2a**. Equivalent results are obtained for **2a** + K^+ (refer to SI section S9.3).



a very low intensity band in the visible range (413 nm and 447 nm). The bathochromic shift observed in the presence of the crown ether is consistent with the expected more important destabilization of the ion pair in the ground state than in the excited state.^{31–33}

As detailed in SI (Section S9), not only the energy but also the nature of the electronic transitions mainly contributing to these two bands are not affected by the presence of K^+ . Indeed in both cases the lower energy band is of Ligand-to-Ligand Charge Transfer (LLCT) character related to an HOMO–LUMO excitation from the two phenolic rings to the ethynylbenzene moiety. The second transition, instead, is essentially a HOMO–LUMO+2 excitation, centred on the aminophenol substituent as depicted in Fig. 6.

The most stable structure computed for the **2a** + **4-FArI** Electron Donor–Acceptor (EDA) complex, exhibiting a π -stacking interaction between **4-FArI** and the aromatic ring linked to the triple bond of **2a** (see SI Section S9.2) was selected among all those generated by an extensive conformational study reported in SI. The absorption spectra computed for this **2a** + **4-FArI** system (see SI, Section S9.3) shows only a slight blue shift (33 nm) with respect to **2a** of the first-low intensity-transition attributed to a destabilization of the LUMO due to stacking interaction.

No additional low-lying spin allowed transitions were observed after the inclusion of the **4-FArI** molecule, ruling out a direct spin allowed light induced CT from **2a** and **4-FArI**. However, a low-lying vertical triplet state is computed both in the case of **2a** and **2a** + **4-FArI** + K^+ (**2a-T₀^{GS}** at 2.7 eV and **2a+4-FArI-T₀^{GS}** at 2.8 eV, respectively in Fig. 7 and Section S9.6). In

both cases, the computed triplet spin density reveals that this triplet corresponds mainly to an excitation from the phosphorous to the ethynylbenzene moiety (Fig. 7).

Relaxation of **2a-T₀^{GS}** and **2a+4-FArI-T₀^{GS}** does not alter the spin localization and the nature of these triplets and leads to **2a-T₀^A** and **2a+4-FArI-T₀^A**, respectively, both located 2.1 eV above the GS. The situation is different for the **2a** + **4-FArI** + K^+ system where the presence of a potassium cation close to the iodine atom leads to a spontaneous break of the C–I bond of **4-FArI** and to the formation of a new K–I electrostatic interaction (see SI for an analysis of NCI, Section S9.7). Actually, even in the absence of the potassium cation, scans along the C–I bond performed on the triplet state revealed a very low barrier for the C–I bond breaking, allowing to identify a lower triplet state also for the **2a** + **4-FArI** system, resting at 1.4 eV above the GS (**2a+4-FArI-T₀^B**) and corresponding to the cleavage of the C–I bond. This explains why the reaction can still occur in the presence of a K^+ scavenger such as the 18-crown-6.

To sum up, these computational insights confirm that a single electron transfer (SET) can occur from the EDA complex **2a** + **4-FArI**, causing a practically barrierless breaking of the Ar–I bond and giving rise to an aromatic radical. This radical can recombine with the radical derived from **2a** to produce **5a**. On the other hand, since the highest spin density is located on the phosphorous atom, two radicals could also recombine to form **3a**. Substitution of the **4-FArI** by phenyl iodide (ArI) did not alter the observed mechanism, demonstrating that the fluorine substitution of the substrate is not responsible of the observed reactivity (for further results regarding the ArI system refer to SI, Section S9).

Finally, to test the influence of the triple bond on the reducing ability of the phosphoranide, the same analysis was performed on the benzyl phosphoranide **2b** (see SI, Section S9). The results obtained, reported in SI, shows that the same SET mechanism observed for **2a** is at work, and that actually the SET should be more favorable since only the triplet corresponding to the dissociative state could be located, as a consequence of its higher reducing ability.

Encouraged by these findings, the reactivity of the two phosphoranides **2a** and **2b** with aryl halides was then investigated under UV-Vis irradiation. When irradiating **2a.18-cr-6** at 450 nm in THF in the presence of 4-fluorophenyl halides in a sealed NMR tube, we observed the formation of fluorobenzene at –114.4 ppm by ^{19}F NMR. The latter most likely resulted from a Hydrogen Atom Transfer (HAT) of a transient aryl radical with the solvent. Consistently with the reduction potential of Ar–X varying according to $Cl < Br < I$, an increasing amount of fluorobenzene was formed when going from aryl chloride to iodide (Fig. 8). However, the reaction requires 48 h to go to completion even for aryl iodides.

Conversely, **2b.18-cr-6** reacted under the same conditions in THF with 4-fluorophenyl iodide and 4-fluorophenyl bromide within 3 h and required 5 h to reach completion with the corresponding chloride (Fig. 9a and Section S4.2). Interestingly, when irradiating a mixture of 1,4-difluorobenzene with **2b.18-cr-6** in THF, we were able to detect the formation of fluorobenzene indicating that the excited anion **2b.18-cr-6** is able to

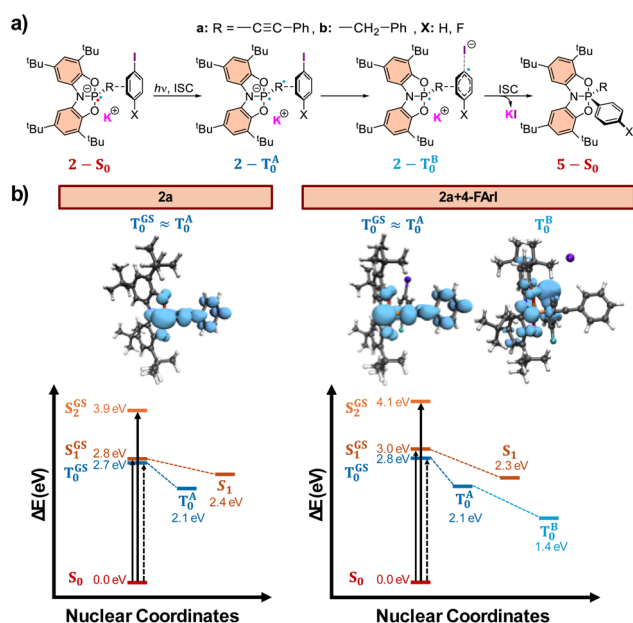


Fig. 7 (a) (Top) SET-mediated mechanism for the formation of **5a** and **5b**. (b) (Top) spin density computed for the optimized triplets of **2a** and **2a** + **4-FArI** systems (isovalue 0.004 a.u.). (Bottom) energy diagram (in eV) GS super indexed states stand for vertical transitions from the GS geometry.

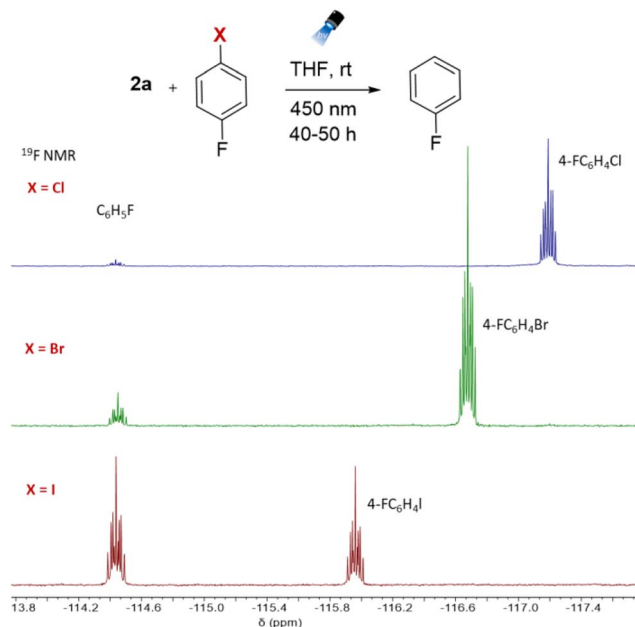


Fig. 8 Reactivity of 2a with ArX under irradiation.

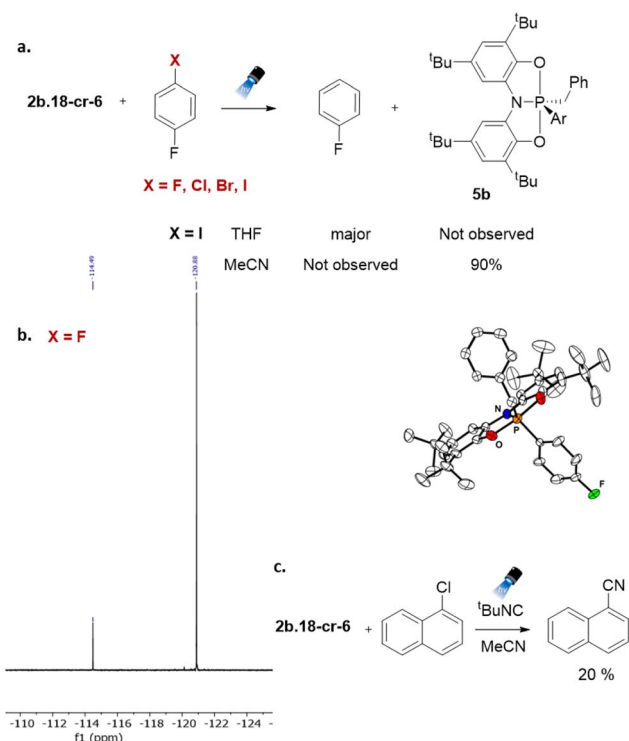


Fig. 9 Reactivity of 2b with ArX under UV-vis irradiation.

reduce aryl fluorides (Fig. 9b). In order to prove the formation of an aryl radical, the reaction of the 4-fluorophenyl iodide with **2b.18-cr-6** was then performed under irradiation in MeCN, less prone to undergo hydrogen atom transfer. In this case, the Ar-P(v) **5b** resulting from the coupling of the aryl radical and the phosphoranyl radical arising from the oxidation of **2b.18-cr-6**

was isolated (Fig. 9a). However, this product was contaminated by the bisbenzyl-P(v) **5b'** (not shown) suggesting that benzyl scrambling occurred in the reaction mixture, presumably due to α -scission of the phosphoranyl radical obtained by photo-induced oxidation of **2b.18-cr-6** (see SI Section S2.3.f). Interestingly, when performing the same reaction with **2a** instead of **2b**, a more complex λ^5 phosphole is formed, which likely results from addition of the phosphoranyl radical onto the triple bond of the expected P(v) product (Fig. S52). This photo-induced radical cascade constitutes a new way to access such complex heterocycles.

The transient sp^2 radical arising from the reduction of 1-chloronaphthalene by the excited **2b.18-cr-6** can also be trapped by *tert*-butyl isocyanide leading to the corresponding 1-naphthalenecarbonitrile in an unoptimized 20% yield (Fig. 9c). All these results confirmed the light-promoted SET between the phosphorane and an acceptor. However, since the UV-vis spectrum of **2b.18-cr-6** shows almost no absorption above 400 nm, these findings strongly support the involvement of an EDA complex as suggested by theoretical studies.

Conclusions

In summary, we have shown that O,N,O-pincer ligated phosphorane anions derived from geometrically constrained P(III) **1** undergo visible-light-induced single-electron transfer reactions with of aryl halides. Their unique electronic properties and the aromatic ONO ligand facilitate the formation of photoexcited electron donor-acceptor complexes, as supported by a combination of experimental observations and theoretical analysis. These findings provide new insight into the photochemical behavior of anionic P(III) constrained main-group species and establish them as valuable platforms for light-driven reactivity.

Author contributions

E. E. and L. B. conducted all the experiments and performed data analysis. M. P. conducted DFT calculations. G. G. performed the X-ray analysis. S. L., M. R. V. and L. G. conceived the project and supervised the experimental work and I. C. supervised the theoretical work. The manuscript was written through contributions of all authors. All authors have given approval to the final version of the manuscript.

Conflicts of interest

There are no conflicts to declare.

Data availability

CCDC 2469381–2469388 contain the supplementary crystallographic data for this paper.^{34a–h}

Supplementary information: experimental procedures; ^1H , ^{13}C , and ^{31}P NMR characterization of new compounds with copies of the corresponding spectra; crystallographic methods and data (deposited at the CCDC, CIF and checkCIF files), and



tabulated coordinates; DFT methods and optimized structures with coordinates. See DOI: <https://doi.org/10.1039/d5sc06960b>.

Acknowledgements

The authors gratefully thank the ANR (ANR-20-CE07-0020, PHOTOFLAT), the CNRS, the ENS-PSL and Sorbonne University for financial support. They also acknowledge N. Touati and L. Binet for helpful and fruitful discussions.

Notes and references

- 1 S. E. Denmark and G. L. Beutner, *Angew. Chem., Int. Ed.*, 2008, **47**, 1560–1638.
- 2 S. Lakhdar, in *Lewis Base Catalysis in Organic Synthesis*, ed. E. Vedejs and S. E. Denmark, Wiley, 2016, pp. 85–118.
- 3 H. Guo, Y. C. Fan, Z. Sun, Y. Wu and O. Kwon, *Chem. Rev.*, 2018, **118**, 10049–10293.
- 4 S. A. Culley and A. J. Arduengo, *J. Am. Chem. Soc.*, 1984, **106**, 1164–1165.
- 5 A. J. Arduengo and C. A. Stewart, *Chem. Rev.*, 1994, **94**, 1215–1237.
- 6 J. Abbeneth and J. M. Goicoechea, *Chem. Sci.*, 2020, **11**, 9728–9740.
- 7 T. P. Robinson, S. Lo, D. De Rosa, S. Aldridge and J. M. Goicoechea, *Chem.–Eur. J.*, 2016, **22**, 15712–15724.
- 8 S. M. McCarthy, Y.-C. Lin, D. Devarajan, J. W. Chang, H. P. Yennawar, R. M. Rioux, D. H. Ess and A. T. Radosevich, *J. Am. Chem. Soc.*, 2014, **136**, 4640–4650.
- 9 H. W. Moon, A. Maity and A. T. Radosevich, *Organometallics*, 2021, **40**, 2785–2791.
- 10 W. Zhao, S. M. McCarthy, T. Y. Lai, H. P. Yennawar and A. T. Radosevich, *J. Am. Chem. Soc.*, 2014, **136**, 17634–17644.
- 11 T. P. Robinson, D. M. De Rosa, S. Aldridge and J. M. Goicoechea, *Angew. Chem., Int. Ed.*, 2015, **54**, 13758–13763.
- 12 J. Abbeneth, O. P. E. Townrow and J. M. Goicoechea, *Angew. Chem., Int. Ed.*, 2021, **60**, 23625–23629.
- 13 M. K. Mondal, L. Zhang, Z. Feng, S. Tang, R. Feng, Y. Zhao, G. Tan, H. Ruan and X. Wang, *Angew. Chem., Int. Ed.*, 2019, **58**, 15829–15833.
- 14 N. Beims, T. Greven, M. Schmidtman and J. I. Van Der Vlugt, *Chem.–Eur. J.*, 2023, **29**, e202302463.
- 15 J. Cui, Y. Li, R. Ganguly, A. Inthirarajah, H. Hirao and R. Kinjo, *J. Am. Chem. Soc.*, 2014, **136**, 16764–16767.
- 16 A. Brand and W. Uhl, *Chem.–Eur. J.*, 2019, **25**, 1391–1404.
- 17 T. J. Hannah and S. S. Chitnis, *Chem. Soc. Rev.*, 2024, **53**, 764–792.
- 18 A. J. King, J. Abbeneth and J. M. Goicoechea, *Chem.–Eur. J.*, 2023, **29**, e202300818.
- 19 S. Volodarsky and R. Dobrovetsky, *Chem. Commun.*, 2018, **54**, 6931–6934.
- 20 D. Roth, J. Stirn, D. W. Stephan and L. Greb, *J. Am. Chem. Soc.*, 2021, **143**, 15845–15851.
- 21 S. Volodarsky, D. Bawari and R. Dobrovetsky, *Angew. Chem., Int. Ed.*, 2022, **61**, 1–8.
- 22 K. Chulsky, I. Malahov, D. Bawari and R. Dobrovetsky, *J. Am. Chem. Soc.*, 2023, **145**(6), 3786–3794.
- 23 D. Bawari, D. Toami, K. Jaiswal and R. Dobrovetsky, *Nat. Chem.*, 2024, **16**, 1261–1266.
- 24 D. Roth, A. T. Radosevich and L. Greb, *J. Am. Chem. Soc.*, 2023, **145**, 24184–24190.
- 25 L. You, D. Roth and L. Greb, *Chem. Sci.*, 2025, **16**, 1716–1721.
- 26 S. Volodarsky, I. Malahov, D. Bawari, M. Diab, N. Malik, B. Tumanskii and R. Dobrovetsky, *Chem. Sci.*, 2022, **13**, 5957–5963.
- 27 J. E. Swartz and J. F. Bunnett, *J. Org. Chem.*, 1979, **44**, 340–346.
- 28 R. A. Rossi, *Acc. Chem. Res.*, 1982, **15**, 164–170.
- 29 S. M. Barolo, S. E. Martin and R. A. Rossi, *Arkivoc*, 2012, 98–106.
- 30 H. Zeng, Q. Dou and C.-J. Li, *Org. Lett.*, 2019, **21**, 1301–1305.
- 31 M. Schmalzbauer, M. Marcon and B. König, *Angew. Chem., Int. Ed.*, 2021, **60**, 6270–6292.
- 32 M. A. Fox, *Chem. Rev.*, 1979, **79**, 253–273.
- 33 J.-P. Soumilion, in *Photoinduced Electron Transfer V*, ed. J. Mattay, Springer, Berlin, Heidelberg, 1993, pp. 93–141.
- 34 (a) CCDC 2469381: Experimental Crystal Structure Determination, 2025, DOI: [10.5517/ccdc.csd.cc2nwlgm](https://doi.org/10.5517/ccdc.csd.cc2nwlgm); (b) CCDC 2469382: Experimental Crystal Structure Determination, 2025, DOI: [10.5517/ccdc.csd.cc2nwlhn](https://doi.org/10.5517/ccdc.csd.cc2nwlhn); (c) CCDC 2469383: Experimental Crystal Structure Determination, 2025, DOI: [10.5517/ccdc.csd.cc2nwljp](https://doi.org/10.5517/ccdc.csd.cc2nwljp); (d) CCDC 2469384: Experimental Crystal Structure Determination, 2025, DOI: [10.5517/ccdc.csd.cc2nwlkq](https://doi.org/10.5517/ccdc.csd.cc2nwlkq); (e) CCDC 2469385: Experimental Crystal Structure Determination, 2025, DOI: [10.5517/ccdc.csd.cc2nwllm](https://doi.org/10.5517/ccdc.csd.cc2nwllm); (f) CCDC 2469386: Experimental Crystal Structure Determination, 2025, DOI: [10.5517/ccdc.csd.cc2nwllms](https://doi.org/10.5517/ccdc.csd.cc2nwllms); (g) CCDC 2469387: Experimental Crystal Structure Determination, 2025, DOI: [10.5517/ccdc.csd.cc2nwllnt](https://doi.org/10.5517/ccdc.csd.cc2nwllnt); (h) CCDC 2469388: Experimental Crystal Structure Determination, 2025, DOI: [10.5517/ccdc.csd.cc2nwlpv](https://doi.org/10.5517/ccdc.csd.cc2nwlpv).

